IEEE Access
Multidisciplinary | Rapid Review | Open Access Journal

Received May 14, 2021, accepted May 26, 2021, date of publication June 3, 2021, date of current version June 15, 2021.

Digital Object Identifier 10.1109/ACCESS.2021.3085557

Repeatability Analysis of an Overconstrained Kinematic Coupling Using a Parallel-Mechanism-Equivalent Model

JIANZHONG DING[1], XUEAO LIU[1], AND CHUNJIE WANG[2]
[1]School of Mechanical Engineering and Automation, Beihang University, Beijing 100191, China
[2]State Key Laboratory of Virtual Reality Technology and Systems, Beihang University, Beijing 100191, China

Corresponding author: Jianzhong Ding (jianzhongd@buaa.edu.cn)

This work was supported by the Joint Fund of Advanced Aerospace Manufacturing Technology Research under Grant U2037602.

ABSTRACT A parallel-mechanism-equivalent model for repeatability analysis of an overconstrained kinematic coupling is proposed. An overconstrained Kelvin-type coupling with one additional support is introduced and used for method illustration. Contact forces of the an overconstrained coupling under a preload are computed with the Moore-Penrose inverse, and the deformations are obtained using the Hertz theory. The coupling is equivalently modeled as a 7-SPS parallel mechanism, the spherical joints of which represent centers of supporting balls and contact points, and prismatic joints are used to simulate the deformations. Therefore, the pose error of the coupling due to a preload is analyzed using the well-appraised incremental method for forward kinematics analysis of parallel mechanisms. The uncertainties of the preload are discussed and a boundary-sampling method is proposed for repeatability analysis. The main contribution of this study lies in the greatly simplified repeatability analysis of overconstrained kinematic couplings by the proposed parallel-mechanism-equivalent model and the boundary-sampling method. Finally, the proposed methods are validated by a case study.

INDEX TERMS Kinematic coupling, kinematics, repeatability, parallel mechanism.

I. INTRODUCTION

Kinematic couplings restrain 6 degrees of freedom between two components and thus provide an effective way to maintain high repeatability. They are generally classified into two types, namely, the Kelvin coupling and the Maxwell coupling, as shown in Fig. 1.

In Fig. 1, the Kelvin coupling on the left forms a tripod, the three spherical surfaces of which rest in a concave tetrahedron, a V-shaped groove and a flat plate. The Kelvin coupling has a nonsymmetric 3-2-1 contact mode. The Maxwell coupling is symmetric, and the three spherical surfaces of the tripod fit into three V-shaped grooves. Both of the couplings can achieve high repeatability [1], and are therefore widely used to clamp components of sensitive equipment, such as optical telescope assemblies [2], [3], antenna panels [4] and high-precision microcontact printing devices [5]. Apart from the traditional Kelvin-type and Maxwell-type couplings, the two components of which are restrained by 6 contact points, quasikinematic couplings [6], [7] and compliant semikinematic couplings [8], [9] with higher accuracy performance are designed and analyzed.

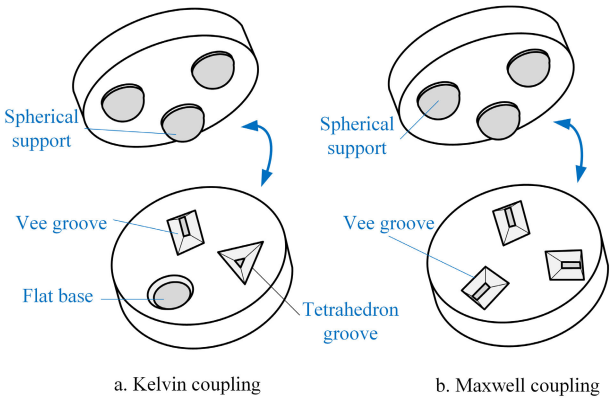

FIGURE 1. Structures of the two classic kinematic couplings.

The associate editor coordinating the review of this manuscript and approving it for publication was Mohammad Alshabi.

For a coupling used to clamp two separate parts, a proper preload is necessary to keep the coupling stable, which inevitably brings in deformations and pose error. Generally, the deformation is computed based on the classical Hertz contact theory [10], [11] and the pose error is obtained by analyzing the motion of rigid bodies in contact. Following this track, Slocum discussed three-groove kinematic coupling design methodologies [10], [11] and proposed several optimization criteria for optimizing kinematic coupling designs [12]. Takagi, Tanaka. and Ishimura [13] studied the effects of pressing order and load on the repeatability of the coupling and obtained the optimal load exerting strategy. Recently, Yuan et al [14] designed a kinematic coupling mechanism and computed its accuracy by homogeneous transformation matrices. In the aforementioned studies, the well-appraised screw theory and Lie group theory were partly used to establish the error model and the efficiency of the methods were proven. It is noteworthy that the effect of friction is usually excluded in the model due to smooth contact surfaces. However, the friction can be considered to enhance the model accuracy. Ahmadizadeh, Shafei and Jafari [15] proposed an regularized method to model the impact-contact mechanism with friction. Moreover, in addition to the widely used Hertz contact model, Ahmadizadeh and Shafei [16] gave an alternative contact model derived by the Gibbs-Appell recursive algorithm, and applied it to the modeling of mechanism motion with revolute–prismatic flexible joints [17], [18]. In this paper, one of the contributions is that a novel parallel-mechanism-equivalent model is proposed for error modeling of the overconstrained kinematic coupling, in which the screw theory and Lie group theory are used for pose estimation, which simplifies the computation.

Generally, a deterministic kinematic coupling has exactly 6 contact points. However, in some specific space vehicle applications, additional contact is used for better stiffness and accuracy, e.g., the kinematic coupling used to clamp components of the James Webb Space Telescope has an overconstrained 3-2-1-1-1-1-1-1 configuration [2], [3]. In this paper, an overconstrained 3-2-1-1 kinematic coupling is discussed and its repeatability considering preload uncertainties is analyzed. We aim to estimate the maximum deviations that may occur in the repeated clamping process. This maximum-searching or boundary-searching problem concerning uncertainties is being studied persistently, and numerous approaches have been developed, such as the optimization method [19], sampling methods [20], [21], interval analysis methods [22], [23] and geometrical methods [24], [25]. In this paper, we combined the sampling approach and interval analysis method for repeatability analysis, which greatly reduced the computational cost on the premise of high accuracy.

The rest of this paper is organized as follows. Section 2 presents a brief introduction of the overconstrained 3-2-1-1 kinematic coupling and discusses the error-pose-estimation method using a parallel-mechanism-equivalent model. In Section 3, a latch device used to exert preload is introduced, following which the uncertainties of preload are discussed. Then, a boundary-sampling method for repeatability analysis is developed. The proposed parallel-mechanism-equivalent model and the boundary-sampling method is validated in Section 4 with a study case, and finally, in Section 5, we conclude our work.

II. PARALLEL-MECHANISM-EQUIVALENT MODEL FOR OVERCONSTRAINED KINEMATIC COUPLING

A. STRUCTURE OF OVERCONSTRAINED KELVIN COUPLING

The overconstrained kinematic coupling scenario discussed in this paper is a Kelvin-type clamp with an additional flat contact between two fixtures, as shown in Fig. 2.

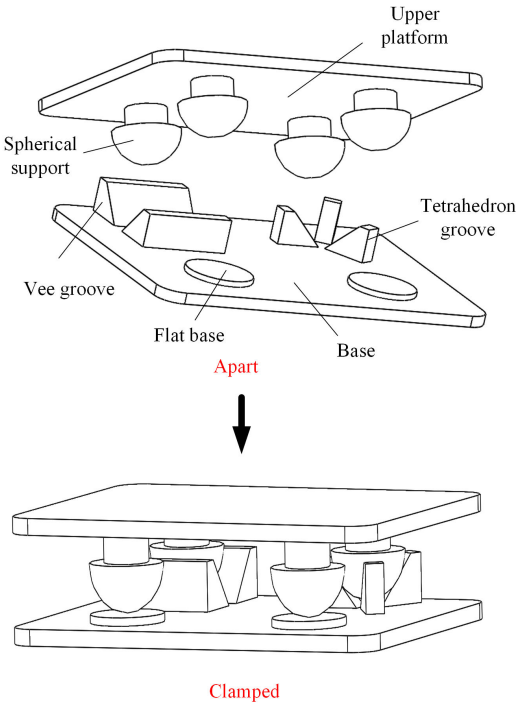

FIGURE 2. Schematic diagram of the Kelvin coupling.

Its corresponding geometric model in the clamped state is then obtained, as shown in Fig. 3.

As shown in Fig. 3, A, B, C and D denote the centers of the contact balls, $A_1, A_2, A_3, B_1, B_2, C_1$ and D_1 are respective contact points. θ_1 and θ_2 indicate the orientations of the tetrahedron and the vee groove, respectively. In this paper, θ_1 is $\pi/3$ and θ_2 is $\pi/2$. Contact surfaces of the tetrahedron and the vee groove are planes with an angle of $\pi/4$ to the XY plane.

B. PARALLEL-MECHANISM-EQUIVALENT (PME) MODEL

A kinematic coupling consists of two separate components, namely, the component with contact spheres and the component with contact planes. Throughout the paper, the component with spheres (hemispheres for the coupling discussed in this paper) is considered moveable and the other component is

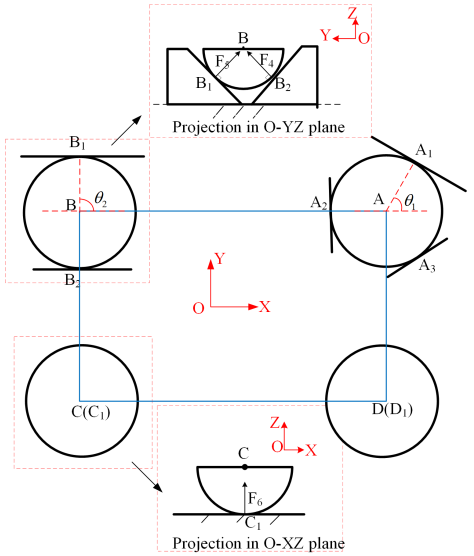

FIGURE 3. Geometric model of the overconstrained Kelvin coupling.

considered to be fixed to the base for description convenience. The PME model is valid based on the following assumptions:

a. All the surfaces of the coupling make contact simultaneously when clamping, and the clamped surfaces remain in contact from then onward.
b. No slip occurs between the contact point and the contact surface.
c. There is no friction between the contact point and the contact surface.
d. The upper platform and the base in Fig. 2 are rigid.

The assumptions guarantee that the pose of the upper platform only changes with respect to deformations of the contact areas. Then, the PME model can be established, as shown in Fig.4.

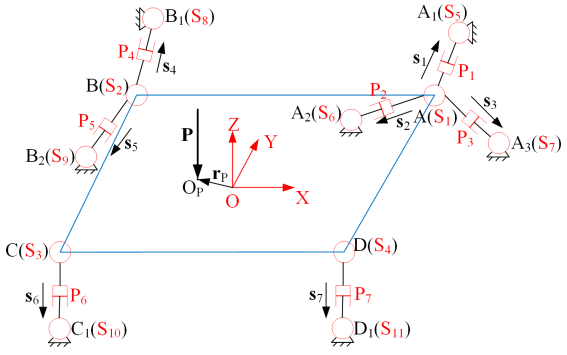

FIGURE 4. PME model for the overconstrained Kelvin coupling.

As shown in Fig. 4, centers of the hemispheres denoted by A, B, C and D are modeled as spherical joints (denoted as S_1, S_2, S_3 and S_4, respectively) connected to the moveable upper platform, contact points $A_1, A_2, A_3, B_1, B_2, C_1$ and D_1 are modeled as spherical joints (denoted as $S_5, S_6, S_7, S_8, S_9, S_{10}$ and S_{11}, respectively) connected to the fixed base, and $P_1, P_2, P_3, P_4, P_5, P_6$ and P_7 denote prismatic joints connecting the upper platform and the base. In this way, a 7-SPS PME model is obtained. Unit vector $\mathbf{s}_i (i = 1, 2, \cdots, 7)$ indicates the direction of the respective prismatic joint. Since the deformation that occurs at each contact is small and its direction is from the contact point to the center of the contact ball, the elastic deformation under preload can be equivalently simulated by a linear movement of each prismatic joint. Moreover, the elastic force is a function of deformation and it can be completely formulated with the translational stroke of the prismatic joint. Therefore, from the motion and force points of view, the proposed PME model can represent kinematic coupling.

C. ERROR MODELING USING THE PME MODEL

Using the proposed PME model, the error model of the overconstrained kinematic coupling can be established with the well-developed forward kinematics analysis methods for parallel mechanisms. Given that a preload $\mathbf{P}$ is exerted on the manipulator at point O_P, and vector $\mathbf{r}_P$ is from the origin of the global coordinate system $O - XYZ$ to the point O_F, as shown in Fig. 4, then, the force $\mathbf{W}$ expressed in the wrench form at O is

$$\mathbf{W} = \begin{pmatrix} \mathbf{P} \\ \mathbf{r}_P \times \mathbf{P} \end{pmatrix}. \tag{1}$$

The opposite direction of the elastic force in each limb is computed as

$$\mathbf{s}_i = \frac{\mathbf{x}_i - \mathbf{y}_i}{\| \mathbf{x}_i - \mathbf{y}_i \|}, \quad i = 1, 2, \cdots 7 \tag{2}$$

where $\mathbf{y}_1 = \mathbf{y}_2 = \mathbf{y}_3$ denote the coordinates of A, $\mathbf{y}_4 = \mathbf{y}_5$ denote the coordinates of B, and $\mathbf{y}_6$ and $\mathbf{y}_7$ denote the coordinates of C and D, respectively. $\mathbf{x}_i$ denotes the coordinate of each contact point and $\| \cdot \|$ computes the Euclidean norm of a vector. Then the balance of the preload and the elastic forces represented at O gives

$$\begin{pmatrix} \mathbf{s}_1 & \cdots & \mathbf{s}_7 \\ \mathbf{r}_{x1} \times \mathbf{s}_1 & \cdots & \mathbf{r}_{x7} \times \mathbf{s}_7 \end{pmatrix} \begin{pmatrix} F_1 \\ F_2 \\ F_3 \\ F_4 \\ F_5 \\ F_6 \\ F_7 \end{pmatrix} = \mathbf{HF} = \mathbf{W}, \tag{3}$$

where $\mathbf{r}_{xi} (i = 1, 2, \cdots, 7)$ is the vector from O to the contact point, and $F_i (i = 1, 2, \cdots, 7)$ is the magnitude of each contact force. $\mathbf{H}$ and $\mathbf{F}$ are the stacks of direction vectors and contact forces, respectively.

For the overconstrained 7-SPS parallel mechanism, $\mathbf{H}$ is a 6×7 matrix with linearly dependent columns. Then the elastic contact force is computed as

$$\mathbf{F} = \mathbf{H}^{+}\mathbf{W}, \tag{4}$$

where $\mathbf{H}^{+}$ is the Moore-Penrose inverse expressed as

$$\mathbf{H}^{+} = (\mathbf{H}^{*}\mathbf{H})^{-1}\mathbf{H}^{*} = (\mathbf{H}^{\top}\mathbf{H})^{-1}\mathbf{H}^{\top}, \tag{5}$$

where the associated matrix $\mathbf{H}^*$ equals the transposed matrix $\mathbf{H}^\top$ since $\mathbf{H}$ is a real matrix. The deformation under each contact force can be computed using Hertz contact theory, as

$$d_{0i} = \left(\frac{3F_i}{4E}\right)^{\frac{2}{3}} \left(\frac{1}{R}\right)^{\frac{1}{3}}, \quad i = 1, 2, \cdots 7 \tag{6}$$

where R is the radius of the contact ball and E is the equivalent moduli of elasticity, as

$$\frac{1}{E} = \frac{1 - v_2^2}{E_1} + \frac{1 - v_2^2}{E_2}, \tag{7}$$

where E_1 and E_2 are the moduli of elasticity of the ball and the contact plane, respectively. v_1 and v_2 are the Poisson's ratios of the ball and the plane, respectively.

It was stated previously that the deformation can be simulated by the one-way translation of the prismatic joint. Therefore, the stroke of each prismatic joint satisfies $d_i = -d_{0i}$. For a parallel mechanism, the pose of the manipulator can be easily computed with small length increments in limbs from the forward kinematics point of view. Connection between small changes in limbs and the manipulator movement can be expressed as [26]

$$d_i = \frac{(\mathbf{x}_i - \mathbf{y}_i)^\top (\mathbf{y}_i\times, -\mathbf{I}_3)}{\| \mathbf{x}_i - \mathbf{y}_i \|}\xi. \tag{8}$$

Stacking d_i and the part before ξ respectively, we have

$$\mathbf{d} = \mathbf{H}_2\xi, \tag{9}$$

where the 6×1 vector $\xi = [e_{r1}, e_{r2}, e_{r3}, e_{t1}, e_{t2}, e_{t3}]^\top$ is a screw indicating the movement of the manipulator that represents the 6-dimensional error of the kinematic coupling. $\mathbf{e}_r = [e_{r1}, e_{r2}, e_{r3}]^\top$ is the 3-dimensional rotation, and $\mathbf{e}_t = [e_{t1}, e_{t2}, e_{t3}]^\top$ is the 3-dimensional translation. $\mathbf{I}_3$ is the 3×3 identity matrix, and $\mathbf{y}_i\times$ computes the skew-symmetric matrix corresponding to $\mathbf{y}_i$. Given that the coordinate $\mathbf{y}_i = [y_{1i}, y_{2i}, y_{3i}]^\top$, the skew-symmetric matrix is formulated as

$$\mathbf{y}_i\times = \begin{pmatrix} 0 & -y_{3i} & y_{2i} \\ y_{3i} & 0 & -y_{1i} \\ -y_{2i} & y_{1i} & 0 \end{pmatrix} \tag{10}$$

Matrix $\mathbf{H}_2$ is a 7×6 matrix with linearly dependent rows, and thus, the screw ξ is computed as

$$\xi = \mathbf{H}_2^+\mathbf{d}, \tag{11}$$

where $\mathbf{H}_2^+$ is the Moore-Penrose inverse expressed as

$$\mathbf{H}_2^+ = \mathbf{H}_2^*(\mathbf{H}_2\mathbf{H}_2^*)^{-1} = \mathbf{H}_2^\top(\mathbf{H}_2\mathbf{H}_2^\top)^{-1}. \tag{12}$$

Since the screw $\xi = [e_{r1}, e_{r2}, e_{r3}, e_{t1}, e_{t2}, e_{t3}]^\top$ obtained by Eq.(11) is as small as $\| \xi \| \ll 1$, the 4×4 homogeneous matrix, which is an element of the Lie group SE(3) indicating 3-dimensional rigid-body movement, can be formulated as

$$g_e = e^{\xi} \approx \begin{pmatrix} 1 & -e_{r3} & e_{r2} & e_{p1} \\ e_{r3} & 1 & -e_{r1} & e_{p2} \\ -e_{r2} & e_{r1} & 1 & e_{p3} \\ 0 & 0 & 0 & 1 \end{pmatrix}. \tag{13}$$

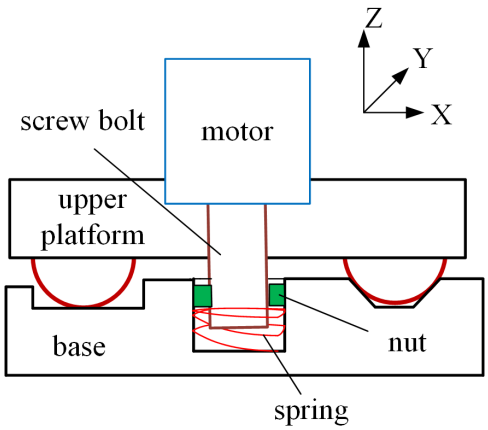

FIGURE 5. Schematic diagram of the preload device.

Then, the clamping error due to the preload can be indicated by ξ, and the error pose of the upper platform is indicated by g_e.

III. REPEATABILITY ANALYSIS WITH PRELOAD UNCERTAINTY

A. PRELOAD UNCERTAINTY ANALYSIS

The preload used to lock the coupling is provided by a latch device, as shown in Fig. 5.

As shown in Fig. 5, the floating nut is in the cylinder of the base and the bolt actuated by a motor is fixed to the upper platform. First, the nut is properly aligned to the driving screw bolt. Then, the motor rotates the bolt and the floating nut is pulled toward the upper platform. When the nut is driven to a proper position, the bolt and the nut are locked together. The spring at the bottom is tensioned and provides the preload to clamp the coupling.

For the preload device, clearance between the floating nut and the cylinder is necessary to achieve the relative motion between them, which may deviate the preload away from the designed $-OZ$ direction. The direction of the preload in practice is restrained in an error cylinder, as shown in Fig. 6.

As shown in Fig. 6, the error cylinder with radius r and height L_1 is used to restrain the preload $\mathbf{P}$, wherein r simulates the clearance and L_1 denotes the distance between the floating nut and the bottom of the cylinder. Then, the real direction of the preload is

$$\mathbf{s}_P = \frac{(r_e \cos\beta, r_e \sin\beta, -L_1)^\top}{\| (r_e \cos\beta, r_e \sin\beta, -L_1)^\top \|} \tag{14}$$

where $r_e \in [0, r]$ and β indicates the direction of r_e.

The preload is exerted by a spring and there could be a deviation in the magnitude of the force. Given that the deviation is below 1% of the designed force according to the manufacturing of springs, the real magnitude of the force satisfies

$$\| \mathbf{P} \| \in \{P | 0.99P_0 \le P \le 1.01P_0\}, \tag{15}$$

where P_0 is the designed magnitude of the preload.

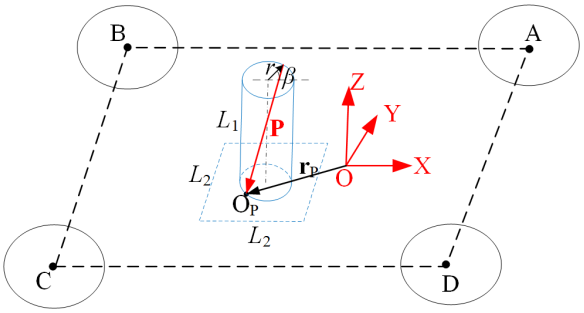

FIGURE 6. Uncertainty of the preload.

Apart from the direction error and magnitude error,there is positioning error at the point of application due to manufacturing and assembling. That is, the point O_P may locate at an arbitrary position within a square region with side length L_2, as shown in Fig. 6. Then we have

$$x_P \in \{x_P | x_{P0} - \frac{L_2}{2} \le x_P \le x_{P0} - \frac{L_2}{2}\} \tag{16}$$

and

$$y_P \in \{y_P | y_{P0} - \frac{L_2}{2} \le y_P \le y_{P0} - \frac{L_2}{2}\}, \tag{17}$$

where $(x_P, y_P)^\top$ and $(x_{P0}, y_{P0})^\top$ denote the coordinates of real and error-free points of application for the preload, respectively.

To conclude, the uncertainties of the preload consist of three parts, namely, the pointing uncertainty, the positioning uncertainty and the magnitude uncertainty.

B. REPEATABILITY ANALYSIS

Generally, the repeatability with load uncertainty is computed by sampling, as

$$\delta_i = \max(\bigcup_{n=1}^{N} \xi_n(i)) - \min(\bigcup_{n=1}^{N} \xi_n(i)), \quad i = 1, 2, \cdots, 6, \tag{18}$$

where $\xi_n(i)$ denotes the i-th entry of the n-th screw ξ_n, and N is the number of samples. As discussed in subsection 3.1, all the errors of the preload are constrained in closed regions with boundaries. Moreover, for the kinematic couplings, the error of the coupling is monotonically correlated with the preload, and thus, we compute the maximum error and the minimum error by only sampling on the boundaries. The accuracy of the simplified boundary-sampling method (BSM) is validated in the following case study section.

In the boundary-sampling method, for the preload direction uncertainty, we set the $r_e = r$ in Eq.(14) and sampling on β in the interval $[0, 2\pi]$. For the magnitude uncertainty, only two situations are considered, namely, $P = 0.99P_0$ and $P = 1.01P_0$. Finally, for the positioning uncertainty, the coordinate of the application point $(x_P, y_P)^\top$ has four choices: that is, they are $(x_{P0} - L_2/2, y_{P0} - L_2/2)^\top$, $(x_{P0} - L_2/2, y_{P0} + L_2/2)$, $(x_{P0} + L_2/2, y_{P0} - L_2/2)$ and $(x_{P0} + L_2/2, y_{P0} + L_2/2)$. Then the repeatability considering preload uncertainties can be obtained by Eq.(18). Finally, design

TABLE 1. Levels of parameters.

Parameters	Levels
X_1(rad)	$(\pi i)/N_\beta \; i = 1, 2, \cdots, 2N_\beta$
X_2(N)	$0.99P_0, 0.99P_0$
X_3(mm)	$x_{P0} - L_2/2, x_{P0} + L_2/2$
X_4(mm)	$y_{P0} - L_2/2, y_{P0} + L_2/2$

TABLE 2. Structural parameter settings.

Parameter	Description	Value
$[x_A, y_A, y_A]^\top$(mm)	coordinates of A	$[80, 60, 0]^\top$
$[x_B, y_B, y_B]^\top$(mm)	coordinates of B	$[-80, 60, 0]^\top$
$[x_C, y_C, y_C]^\top$(mm)	coordinates of C	$[-80, -60, 0]^\top$
$[x_D, y_D, y_D]^\top$(mm)	coordinates of D	$[80, -60, 0]^\top$
θ_1(rad)	orientation of the tetrahedron	$\pi/3$
θ_2(rad)	orientation of the vee groove	$\pi/2$
R(mm)	radius of the contact ball	30

parameters are selected as $\mathbf{X} = [X_1, X_2, X_3, X_4]^\top$, where $X_1 = \beta$, $X_2 = P$, $X_3 = x_P$ and $X_4 = y_P$. The optimal Latin Hypercube design is used to generate the samples. Levels of parameters are presented in Table 1.

The $2N_\beta$ indicates the sample number of angle β.

IV. METHOD VALIDATION AND CASE STUDY

A. VALIDATION OF THE PROPOSED PME MODEL

A study case is used here to illustrate and verify the proposed PME model and repeatability analysis method. The structure of the overconstrained Kelvin coupling is as shown in Fig. 3 and necessary parameters are given in Table 2.

The contact balls and supports are made of Ti alloy, the elastic modulus ($E_1 = E_2$) of which is 210,000 MPa and the Poisson's ratio of which is 0.3. When the preload $\mathbf{P} = [0, 0, -2600]^\top$ is employed at point O, as shown in Fig. 3, the resultant force expressed in the $O - XYZ$ is formulated as

$$\mathbf{t}_F = \begin{pmatrix} \mathbf{s}_1 & \cdots & \mathbf{s}_7 \\ \mathbf{r}_{x1} \times \mathbf{s}_1 & \cdots & \mathbf{r}_{x7} \times \mathbf{s}_7 \end{pmatrix} \begin{pmatrix} F_1 \\ F_2 \\ F_3 \\ F_4 \\ F_5 \\ F_6 \\ F_7 \end{pmatrix} - \mathbf{W}. \tag{19}$$

When all the forces are balanced, we have $\mathbf{t}_F \to \mathbf{0}$. To verify the accuracy of the PME model, the length deviation of each equivalent limb is computed. Taking limb AA_1 as an example, the length deviation with pose error g_e is

$$\delta d_1 = \| g_e \cdot \mathbf{A} - \mathbf{A}_1 \| - \| \mathbf{A} - \mathbf{A}_1 \| \tag{20}$$

where g_e is the error matrix formulated by Eq.(13), and $\mathbf{A}$ and $\mathbf{A}_1$ denote the coordinates of points A and A_1, respectively, as shown in Fig. 3. Obviously, the PME model is accurate when the length δd_icomputed with g_e equals the deformation d_{0i}. Then, the variable indicating the accuracy of the PME model is defined as

$$\mathbf{t}_G = [\delta d_1 - d_{01}, \delta d_2 - d_{02}, \cdots, \delta d_7 - d_{07}]^\top \tag{21}$$

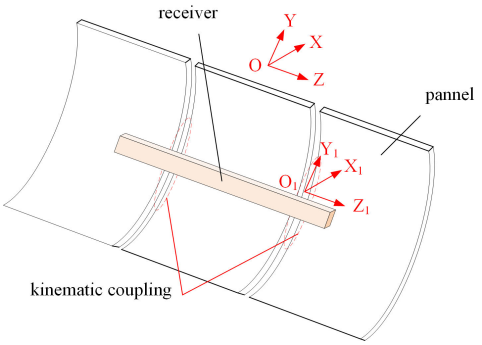

FIGURE 7. Parabolic cylindrical antenna connected by couplings.

After computation, we have

$$\xi = 10^{-4} \times \begin{pmatrix} -2.1219 \\ -0.4127 \\ -83.21 \\ 0.0138 \\ -0.0071 \\ 0 \end{pmatrix} \text{(mm, rad)} \tag{22}$$

$$\mathbf{t}_F = 10^{-11} \times \begin{pmatrix} 0.0003 \\ 1.5220 \\ -0.1364 \\ 0.9549 \\ -2.3647 \\ -0.083 \end{pmatrix} \text{(N)} \tag{23}$$

$$\mathbf{t}_G = 10^{-5} \times \begin{pmatrix} -2.5803 \\ -2.5803 \\ -2.5803 \\ 4.0086 \\ 4.0086 \\ -5.5776 \\ -5.5776 \end{pmatrix} \text{(mm)} \tag{24}$$

It can be seen from Eqs.(22) - (24) that $\mathbf{t}_F \rightarrow 0$ and the error in length deviation is smaller than 10^{-4} mm, suggesting that the proposed PME method for the overconstrained coupling is of high accuracy.

B. REPEATABILITY ANALYSIS OF AN OVERCONSTRAINED KELVIN COUPLING

The overconstrained Kelvin coupling introduced in this paper is used to dock panels of a parabolic cylindrical antenna, as shown in Fig. 7, where $O - XYZ$ is a global coordinate system and $O_1 - X_1Y_1Z_1$ is a local coordinate system used to evaluate the accuracy of an overconstrained kinematic coupling.

As shown in Fig. 7, the panel in the middle is fixed to the satellite. The coplanarity of the three panels has a great effect on the performance of the antenna, and therefore, kinematic couplings are used. The parameters of the overconstrained Kelvin coupling are the same as those in Table 2. The repeatability of the kinematic coupling is analyzed using the BSM discussed in subsection 3.2. Necessary parameters are presented in Table 3.

TABLE 3. Settings of parameters.

Parameters	values
N_β	12
P_0(N)	2600
$[x_{P0}, y_{P0}]^\top$(N)	$[0, 0]^\top$
r(mm)	1
L_2(mm)	1

TABLE 4. Settings of parameters for MCS.

Parameter	Distribution	settings
P(N)	uniform	$U(0.9P_0, 1.1P_0)$
x_{P0}(mm)	uniform	$U(-1, 1)$
y_{P0}(mm)	uniform	$U(-1, 1)$
r(mm)	uniform	$U(-1, 1)$
L_2(mm)	uniform	$U(-1, 1)$

TABLE 5. Results of the repeatability analysis.

Variable	BSM	MCS
δ_1(rad)	$5.5440e-6$	$5.4512e-6$
δ_2(rad)	$3.8239e-6$	$3.7414e-6$
δ_3(rad)	$8.2978e-6$	$8.2386e-6$
δ_4(mm)	$2.5594e-3$	$2.5525e-3$
δ_5(mm)	$1.0117e-3$	$1.0016e-3$
δ_6(mm)	$1.1280e-3$	$1.1247e-3$

The results of the repeatability analysis are validated using Monte Carlo simulation. The parameter settings for the Monte Carlo simulation (MCS) are given in Table 4.

We use 192 samples with the BSM and 10,000 samples with the MCS method, and the results are presented in Table 5.

In Table 5, δ_1,δ_2 and δ_3 are the rotational repeatability errors, and δ_4, δ_5 and δ_6 are the translational repeatability errors. It can be observed from Table 5 that the results computed by MCS are slightly smaller than those obtained by the proposed BSM, suggesting that the proposed BSM is accurate and efficient.

V. CONCLUSION

This paper provides a new way to estimate the pose error of kinematic coupling under preloads. In the proposed method, each deformation movement is simulated by the motion of an SPS limb and the coupling is modeled as a 6-DOF parallel mechanism. Thereafter, uncertainties of the preload are analyzed, and a boundary-sampling strategy for repeatability analysis is developed. Both the PME model and the BSM are verified in the case study of an overconstrained Kelvin kinematic coupling.

The proposed PME model is superior to other approaches because the advanced screw theory can thus be applied for pose analysis. In this paper, a complex overconstrained coupling is used to show the merits of the method. However, the PME model is also feasible for general couplings with exactly 6 restraining contacts. Moreover, the precondition that all surfaces are supposed to be in contact simultaneously can be removed to use the PME model when defects in manufacturing are considered. In this case, an additional judgment algorithm is required to activate the modeling of each SPS limb.

In this study, the effects of slip and friction are not included in the contact model. However, in order to enhance the accuracy of the analysis, contact modeling methods concerning friction can be studied in future work.

REFERENCES

[1] A. Slocum, "Kinematic couplings: A review of design principles and applications," *Int. J. Mach. Tools Manuf.*, vol. 50, no. 4, pp. 310–327, Apr. 2010.
[2] P. Reynolds, C. Atkinson, and L. Gliman, "Design and development of the primary and secondary mirror deployment systems for the cryogenic JWST," in *Proc. 37th Aerosp. Mech. Symp., Johnson Space Center*, May 2004.
[3] B. J. Bos, J. M. Howard, P. J. Young, R. Gracey, L. T. Seals, R. G. Ohl, M. C. Clampin, G. G. Fazio, H. A. Macewen, and J. M. Oschmann, "Global alignment optimization strategies, procedures, and tools for the James Webb space telescope (JWST) integrated science instrument module (ISIM)," *Proc SPIE*, vol. 8442, Sep. 2012, Art. no. 84423I.
[4] V. I. Bujakas, "Kinematic couplings for assemblage and deployment of multi-mirror space reflectors and analogies from the classical optics," *Tech. Phys.*, vol. 63, no. 11, pp. 1646–1655, Nov. 2018.
[5] C. A. Trinkle and L. P. Lee, "High-precision microcontact printing of interchangeable stamps using an integrated kinematic coupling," *Lab Chip*, vol. 11, no. 3, pp. 455–459, 2011.
[6] M. L. Culpepper, "Design of quasi-kinematic couplings," *Precis. Eng.*, vol. 28, no. 3, pp. 338–357, Jul. 2004.
[7] M. L. Culpepper, A. H. Slocum, F. Z. Shaikh, and G. Vrsek, "Quasi-kinematic couplings for low-cost precision alignment of high-volume assemblies," *J. Mech. Design*, vol. 126, no. 3, pp. 456–463, May 2004.
[8] M. An, L. Zhang, S. Xu, and J. Dong, "Design, analysis, and testing of kinematic mount for astronomical observation instrument used in space camera," *Rev. Sci. Instrum.*, vol. 87, no. 11, pp. 1–18, 2016.
[9] B. Liu, W. Wang, Y. Qu, X. Li, X. Wang, and H. Zhao, "Design of an adjustable bipod flexure for a large-aperture mirror of a space camera," *Appl. Opt.*, vol. 57, no. 15, pp. 4048–4055, 2018.
[10] A. H. Slocum, "Kinematic couplings for precision fixturing—Part I: Formulation of design parameters," *Precis. Eng.*, vol. 10, no. 2, pp. 85–91, Apr. 1988.
[11] A. H. Slocum, "Design of three-groove kinematic couplings," *Precis. Eng.*, vol. 14, no. 2, pp. 67–76, Apr. 1992.
[12] L. C. Hale and A. H. Slocum, "Optimal design techniques for kinematic couplings," *Precis. Eng.*, vol. 25, no. 2, pp. 114–127, Apr. 2001.
[13] K. Takagi, H. Tanaka, and K. Ishimura, "Strategy and demonstration of latch mechanisms with kinematic coupling for precise deployable structures," *Trans. Jpn. Soc. Aeronaut. SPACE Sci., Aerosp. Technol. Jpn.*, vol. 17, no. 5, pp. 583–588, 2019.
[14] Y. Ye, L. Chen, L. Yang, J. Dong, S. Xu, and S. Wang, "Precision of kinematic coupling mechanism for optical instruments," *Optik*, vol. 202, Feb. 2020, Art. no. 163592.
[15] M. Ahmadizadeh, A. M. Shafei, and R. Jafari, "Frictional impact-contacts in multiple flexible links," *Int. J. Struct. Stability Dyn.*, vol. 21, no. 6, Jun. 2021, Art. no. 2150075.
[16] M. Ahmadizadeh, A. M. Shafei, and M. Fooladi, "A recursive algorithm for dynamics of multiple frictionless impact-contacts in open-loop robotic mechanisms," *Mechanism Mach. Theory*, vol. 146, Apr. 2020, Art. no. 103745.
[17] M. H. Korayem and S. F. Dehkordi, "Derivation of motion equation for mobile manipulator with viscoelastic links and revolute–prismatic flexible joints via recursive Gibbs–Appell formulations," *Robot. Auto. Syst.*, vol. 103, pp. 175–198, May 2018.
[18] M. H. Korayem, A. M. Shafei, and S. F. Dehkordi, "Systematic modeling of a chain of N-flexible link manipulators connected by revolute–prismatic joints using recursive Gibbs-Appell formulation," *Arch. Appl. Mech.*, vol. 84, no. 2, pp. 187–206, Feb. 2014.
[19] J. Meng, D. Zhang, and Z. Li, "Accuracy analysis of parallel manipulators with joint clearance," *J. Mech. Design*, vol. 131, no. 1, Jan. 2009, Art. no. 011013.
[20] X. Li, X. Ding, and G. S. Chirikjian, "Analysis of angular-error uncertainty in planar multiple-loop structures with joint clearances," *Mechanism Mach. Theory*, vol. 91, pp. 69–85, Sep. 2015.
[21] S. Briot and I. A. Bonev, "Accuracy analysis of 3-DOF planar parallel robots," *Mechanism Mach. Theory*, vol. 43, no. 4, pp. 445–458, Apr. 2008.
[22] R. Yao, W. Zhu, and P. Huang, "Accuracy analysis of stewart platform based on interval analysis method," *Chin. J. Mech. Eng.*, vol. 26, no. 1, pp. 29–34, Jan. 2013.
[23] M. H. F. Kaloorazi, M. T. Masouleh, and S. Caro, "Collision-free workspace of parallel mechanisms based on an interval analysis approach," *Robotica*, vol. 35, no. 8, pp. 1747–1760, Aug. 2017.
[24] G. Chen, H. Wang, and Z. Lin, "A unified approach to the accuracy analysis of planar parallel manipulators both with input uncertainties and joint clearance," *Mechanism Mach. Theory*, vol. 64, no. 6, pp. 1–17, Jun. 2013.
[25] J. Ding, S. Lu, T. Da, C. Wang, and G. S. Chirikjian, "Error space estimation of 3-DoF planar parallel mechanisms," *J. Mech. Robot.*, vol. 11, no. 3, 2019, Art. no. 031013.
[26] Y. Wang, "A direct numerical solution to forward kinematics of general Stewart-Gough platforms," *Robotica*, vol. 25, no. 1, p. 121, 2007.

JIANZHONG DING received the B.C. degree from the Chinese University of Petroleum, Beijing, China, in 2013, and the Ph.D. degree in mechanical engineering from Beihang University, Beijing, in 2019. He is currently a Postdoctoral Researcher with the School of Mechanical Engineering and Automation, Beihang University. His research interests include kinematics, space mechanisms, multi-body dynamics, and simulation.

XUEAO LIU received the B.C. degree from Anhui Jianzhu University, Anhui, China, in 2013, and the M.S. degree from the North China University of Technology, Beijing, China, in 2016. He is currently pursuing the Ph.D. degree with the School of Mechanical Engineering and Automation, Beihang University. His research interests include linkage synthesis, mechanism design, compliant mechanisms, and finite element simulation.

CHUNJIE WANG received the Ph.D. degree in mechanical engineering from the China University of Mining and Technology, Beijing, China, in 1997.

From 1997 to 1999, she was a Postdoctoral Researcher with the School of Mechanical Engineering and Automation, Beihang University, Beijing. Since 1999, she has been a Professor with Beihang University and a member of the State Key Laboratory of Virtual Reality Technology and Systems, Beihang University. Her research interests include digital design and simulation for space mechanisms and structures, multidisciplinary optimization, and reliability analysis of mechanical products.